Ethylene Emission in the Aftermath of Saturn's 2010 Northern Storm

Brigette E. Hesman[a], G.L. Bjoraker[b], R.K. Achterberg[a], P.V. Sada[c], P.N. Romani[b], D.E. Jennings[d], A.W. Lunsford[e], J. Sinclair[f], J. Hurley[f], L.N. Fletcher[f], R.J. Boyle[g], A.A. Simon[h], P.G.J. Irwin[f], F.M. Flasar[b]

[a]*Department of Astronomy, University of Maryland, College Park, MD 20742, USA.*
[b]*NASA/Goddard Spaceflight Center, Code 693, Greenbelt, Maryland, 20771, USA*
[c]*Departamento de Física y Matemáticas, Universidad de Monterrey, Garza García, NL 66238, México*
[d]*NASA/Goddard Spaceflight Center, Code 553, Greenbelt, Maryland, 20771, USA*
[e]*Department of Physics, Catholic University of America, Washington, DC 20064, USA*
[f]*Atmospheric, Oceanic & Planetary Physics, Department of Physics, University of Oxford, Clarendon Laboratory, Parks Road, Oxford, OX1 3PU, UK*
[g]*Department of Physics and Astronomy, Dickinson College, Carlisle, PA 17013, USA*
[h]*NASA/Goddard Spaceflight Center, Code 690, Greenbelt, Maryland, 20771, USA*

Abstract

Saturn's northern storm of 2010-2011 was continuously monitored by instruments aboard the Cassini spacecraft, allowing the opportunity to study this storm system in the infrared to a level never before possible by utilizing Cassini's Composite Infrared Spectrometer (CIRS). Ethylene has been tracked at the millibar altitude level (stratosphere) over the full time frame of this storm. Additional monitoring was provided by the ground-based spectrometer Celeste at the United Kingdom Infrared Telescope (UKIRT) and the NASA Infrared Telescope Facility (IRTF). The time series of these observations finds that ethylene is enhanced at the millibar level over pre-storm levels at temperatures greater than 180 K and remains enhanced in the storm system until temperatures relax back to approxi-

Email address: brigette.e.hesman@nasa.gov (Brigette E. Hesman)

mately the same temperature regime. The resulting maps of ethylene show that ethylene morphology is different from methane morphology and that the ethylene abundances at 1.3 mbar range from 20 ppb to 100 ppb before disappearing by April 2012. The temperatures at the millibar altitude level in this time frame went from the pre-storm 140K to 220K in May 2011, but had only relaxed back to 180K by April 2012. Gas phase chemistry and dynamics have not been able to explain the enhanced ethylene abundances and other sources such as heterogeneous chemistry involving Saturn's stratospheric haze may need to be considered as possible sources of the enhanced ethylene.

Keywords: Saturn, atmosphere, Atmospheres, composition, Atmospheres, structure, Abundances, atmospheres, Atmospheres, chemistry

1. Introduction

Saturn's northern storm of 2010-2011 has presented an excellent opportunity to study one of these rare convective events that occur intermittently in Saturn's northern hemisphere. This storm is only the sixth of its magnitude to ever be observed and the first one at this latitude in over a century. Saturn is known to have massive storm systems that erupt approximately once per saturnian year (29.4 Earth years); typically near the equator, the previous began in September 1990 at 12°N (Sanchez-Lavega et al., 1991; Beebe et al., 1992). In December 2010 Saturn's northern hemisphere was spectacularly disrupted from its slow springtime warming by a massive storm eruption at approximately 40°N (all coordinates given in planetographic latitude in this article) (Fischer et al., 2011). Cassini and ground-based observations of this storm have resulted in a wealth of data. Studying this storm across a large wavelength region has produced a 4-dimensional view

(longitude, latitude, altitude, and time) of the storm and the effect it has had on the surrounding atmosphere. The onset of the storm was first identified by radio emissions, Saturn Electrostatic Discharges (SEDs), measured by the Radio and Plasma Wave System (RPWS) on Cassini; SEDs and lightning likely occur at the depths of the water clouds (Fischer et al., 2011). The tropospheric convective storm clouds that were being fed from below (Sromovsky et al., 2013) between December 2010 and August 2011 were studied in the optical from the ground-based telescopes and Cassini's Imaging Science Subsystem (ISS) (Fischer et al., 2011; Sánchez-Lavega et al., 2011, 2012; Sayanagi et al., 2013). Two heated regions in the stratosphere, referred to as "beacons", which are thought to be the result of waves generated in response to the storm clouds punching through to the upper troposphere, have been monitored in the infrared by Cassini and ground-based telescopes. This has resulted in the discovery of the greatest atmospheric temperature change ever seen on Saturn in addition to unexpected changes in species abundances (Hesman et al., 2012; Fletcher et al., 2012).

Storms on Saturn probe the deep atmosphere as material is transported from levels beyond the reach of sunlight up to the observable atmosphere. Storms have a dramatic effect on the local environment, introducing sudden changes that dwarf the effects of seasonal change as Saturn progresses through its 29-year revolution about the Sun. It is not known what triggers these large storms. The approximate annual periodicity suggests solar forcing, yet sunlight does not reach the water cloud where these storms are believed to originate (Dyudina et al., 2010; Hueso and Sánchez-Lavega, 2004). Saturn radiates more energy than it receives from the Sun, but the details of this process are not well understood. Storms may be a way in which Saturn releases its excess thermal energy in sudden bursts, rather

than gradually. The convective plume that erupted in December 2010 was nearly 10 years earlier than expected in the cycle of great eruptions on Saturn (Sanchez-Lavega et al., 1991). This convective plume was sheared to the north and south by the prevailing wind field. By August 2011 convective activity had largely ceased. However, Saturn's stratosphere remained perturbed by the storm at mid-northern latitudes throughout 2011 and 2012.

Optical studies of these storms provide important information on morphology and cloud top locations as is detailed in Sánchez-Lavega et al. (2012) and Sayanagi et al. (2013). Thermal infrared studies provide additional information on the temperature and gas composition of the environment inside and adjacent to storm systems on Saturn. An early study of the infrared signature of the storm by Fletcher et al. (2011) showed the initial appearance of the beacons in Saturn's stratosphere in January 2011. At this time, a temperature difference of 16 K was observed from the quiescent pre-storm conditions. Between January and April 2011, the tropospheric vortex was flanked by these two stratospheric beacons and temperatures in the beacons continued to rise during this period. In May 2011 the two beacons merged into one resulting in a vortex 80 K warmer than pre-storm conditions (Fletcher et al., 2012; Hesman et al., 2012). Hydrocarbon emission was greatly enhanced, resulting in the detection of stratospheric ethylene emission for the first time by Cassini's Composite Infrared Spectrometer (CIRS) (Hesman et al., 2012).

Previous infrared studies of Saturn's ethylene emission have shown it to be difficult to detect on Saturn (Encrenaz et al., 1975; Bézard et al., 2001), but the high temperatures found in the beacon region in May 2011 produced strong thermal emission at 10.5 μm (950 cm^{-1}) due to ethylene in the stratosphere. Ethylene

is an important species to study as it is a short-lived tracer of photochemistry in Saturn's stratosphere. Stellar occultation data acquired in 2006 by the Ultraviolet Imaging Spectrograph (UVIS) on Cassini yielded a detection and vertical profile of ethylene with a retrieved mole fraction of $1.6\text{x}10^{-9}$ at 0.5 mbar in Saturn's atmosphere at 15.2°N (Shemansky and Liu, 2012) in the pre-storm Saturn. The UVIS observations are very important as ethylene has not been detectable in pre-storm conditions by CIRS and this UVIS measurement provides a pre-storm basis of comparison with the ethylene profile derived from the beacon. This short-lived hydrocarbon is a tracer of chemistry occurring in an unusual dynamical region of Saturn's stratosphere. Ethylene does not reach the deep atmosphere of Saturn and hence the unexpected emission cannot be the result of direct upwhelling. In addition to observing ethylene using CIRS the ground-based cryogenic echelle grating spectrometer, Celeste, was used at a higher spectral resolution to detect a band of ethylene lines in the beacon in May 2011. Using CIRS data we derived a C_2H_4 mole fraction of $0.59 \pm 0.45\text{x}10^{-6}$ at 0.5 mbar and using Celeste data we obtained a mole fraction of $2.7 \pm 0.45\text{x}10^{-6}$ at 0.1 mbar (Hesman et al., 2012). This is two orders of magnitude higher than the amount measured by UVIS prior to the storm. It is also much higher than predicted by photochemical models, indicating that perhaps another production mechanism is required or a loss mechanism is being inhibited. The enhanced ethylene emission could not be explained completely by transport of ethylene from its production at higher altitudes to the altitudes where these measurements are sensitive (Hesman et al., 2012). In the sections that follow, ethylene emission throughout 2011 and 2012 is investigated from ground-based observations using Celeste and using multiple data sets from CIRS. Tracking the changes and morphology of ethylene emission in the beacon

provides insight into the species lifetime and how it responds to temperature in this disturbed region of the atmosphere.

2. Observations

2.1. Spacecraft Observations: CIRS

Heated regions of Saturn's stratosphere at the latitude of the northern storm and confined to 20 to 30 degrees of longitude were first detected by Fletcher et al. (2011). These "beacon" features are thought to be produced by wave activity generated by the massive storm at 40°N latitude extending over a large altitude range from the water cloud near 10 bars to the upper troposphere around 100 mbars. These hot regions were observed regularly using both Cassini and ground-based telescopes at wavelengths in the thermal infrared. Specifically, the combination of Cassini/CIRS observations and ground-based data collected using the spectrometer Celeste provides a powerful set of capabilities for studying hydrocarbons on Saturn. CIRS provides broad-band, absolutely calibrated spectra at high spatial resolution and modest spectral resolution (Flasar et al., 2005). It also provides, through measurements of CH_4 and collision induced H_2 opacity, temperature profiles for both the stratosphere and upper troposphere of Saturn. The use of a cryogenic grating spectrometer (Celeste) operating at resolving powers of up to 30,000 on ground-based telescopes permits the detection of multiple emission lines of ethylene. To investigate ethylene emission in the beacon eleven CIRS data sets with sufficient spectral resolution and longitude coverage were identified. In addition, two ground-based Celeste data sets were collected to monitor the changes in ethylene emission at higher spectral resolution. These observations, along with the initial detection of ethylene by CIRS and Celeste in May 2011 (Hesman et al.,

2012), characterize the changes in ethylene emission throughout 2011 and 2012.

CIRS is a dual Fourier transform spectrometer covering the thermal infrared with three focal planes: the far-infrared focal plane, FP1, which is a single thermocouple detector covering 10-600 cm^{-1}, and two mid-infrared focal planes, FP3 and FP4, which are arrays of 10 HgCdTe detectors covering 600-1100 cm^{-1} and 1100-1500 cm^{-1} respectively (Flasar et al., 2005). The far-infrared detector operates at the instrument temperature of 170 K, and the mid-infrared detectors operate at 80 K. The fields-of-view per detector are 3.9 mrad for the far-infrared and 0.3 mrad for the mid-infrared. The apodized spectral resolution is selectable from 0.5 to 15 cm^{-1}. Only FP3 and FP4 have been used in this study.

There were two types of CIRS observations identified for this study. Observations with a spectral resolution of 0.5 cm^{-1} which sit-and-stare at the planet as it rotates beneath are used to study composition (called COMPSITs). These observations are either performed on the central meridian (low to moderate emission angle) or offset to one of the limbs (high emission angle) with the FP3/FP4 focal planes oriented north-south. COMPSITs at high emission angle have contribution functions for temperature and composition that peak near the 1.0 mbar level in Saturn's stratosphere. Observations with a spectral resolution of 3.0 cm^{-1} which sit-and-stare at the planet as it rotates beneath are used to map temperature and composition (called MIRMAPs). These observations are performed on the central meridian (low to moderate emission angle) in order to obtain temperatures throughout the stratosphere and in the upper troposphere. All CIRS data sets were calibrated using a database that incorporates large amounts of deep space spectra.

Cylindrical maps of radiance (expressed in brightness temperature) in the methane band (1305 cm^{-1}) as well as in the peak of the ethylene band (~950 cm^{-1})

are shown in respectively, Figures 1 and 2. The observations that these maps are created from are detailed in Table 1. These six maps show the methane and ethylene emission in March 2011 (Figs 1& 2a), July 2011 (Figs. 1& 2b) and 1& 2c), December 2011 (Figs. 1& 2d), January 2012 (Figs. 1& 2e), and February 2012 (Fig. 1& 2f). It is clear that in March 2011 there were two hot regions in the stratosphere (as shown in the methane map; Fig. 1a) and a slight hint of ethylene in the more northern hot spot (Fig. 2a). The equivalent map for May 2011 is shown in Hesman et al. (2012). The May 2011 map showed that the two beacons had merged into one and that ethylene emission had "turned-on". The methane and ethylene showed different structure in their beacon shape. By July 2011 the methane maps show that the beacon temperature was dropping and the ethylene beacon was growing more compact. By early 2012 the beacon has dropped by about 50 K from its peak temperature in May 2011 (~220 K) and the ethylene emission has become a small circular feature that is less than 10 degrees in longitude extent compared to its 25 degree longitude extent in May 2011. In addition, the ethylene peak moves from approximately 40°N to 35°N between 2011 and 2012. There was insufficient signal-to-noise (SNR) in the maps in order to map the ethylene abundance over the beacon region. Therefore, all CIRS spectra in a 6° north-south by 20° east-west bin were averaged over the peak ethylene emission region in order to increase the SNR and create a single "hot-spot" spectrum for each of the data sets listed in Table 1. The average longitude, latitude, and emission angle of the binned data is also given in the table. As these observations vary widely in emission angle it is not useful to directly compare their spectra but instead we compare the temperature and ethylene profiles retrieved from these data sets. This is discussed in Section 3.

2.2. *Groundbased Observations: Celeste*

Our ground-based instrument, Celeste, is a cryogenic grating spectrometer with an array detector that can achieve resolving powers up to 30,000. This instrument has been described in Jennings et al. (2009). The instrument setup was similar to that used in previous observations (Romani et al., 2008; Hesman et al., 2009). The Celeste observations were performed at the United Kingdom Infrared Telescope (UKIRT) on July 18, 2011 (DOY = 199) and the NASA Infrared Telescope Facility (IRTF) on April 2, 2012 (DOY = 93). At both UKIRT and the IRTF the spectrometer was coupled to the telescope with foreoptics which provided an approximately f/8 beam to the spectrometer entrance slit. The spectrometer uses an 18 x 34 cm^2 echelle grating and an Si:As detector array with a 128 x 128 pixel format and a spatial resolution of ~0.36″/pixel at UKIRT and 0.82″/pixel at IRTF. The entire spectrometer is cooled with liquid helium to an operating temperature of 6 K.

At both telescopes a 300 μm-wide and 6 mm-long slit was used to capture the spectra. At UKIRT the width corresponds to ~1.5″ in the sky and at the IRTF this is ~3.3″. In both instances the length of the slit is much larger than the size of the planet (equatorial diameter ~17″ at UKIRT and ~19″ at the IRTF) so therefore the length of the slit was oriented in an east-west direction centered on 35°N latitude on Saturn so as to simultaneously cover all the longitudes available corresponding to the storm beacon latitude. In this way each resolution element subtended ~12.5° in latitude (slit width) and 2.6° in longitude (along the slit) at UKIRT, and ~21° in latitude (slit width) and ~6° in longitude (along the slit) at the IRTF. These values are considered for the central meridian of the planet. As we move along the slit towards both limbs the curvature of the planet increases both

of these values per resolution element. In order to further increase the signal-to-noise level of the spectra five spatial pixels were combined for the UKIRT data and four spatial pixels were combined for the IRTF data. This resulted in an effective resolution element of ~12.5° in latitude by ~13° in longitude at UKIRT and ~21° in latitude by ~24° in longitude at the IRTF. This technique was used to guarantee continuous coverage of the beacon as it moved across the dayside hemisphere of Saturn. At both telescopes this slit width yields a spectral resolution of ~0.1 cm^{-1}, and the detector array covers a ~2 cm^{-1} spectral interval centered on 949.6 cm^{-1} at UKIRT and 949.4 cm^{-1} at the IRTF.

Sky subtraction was performed by regularly chopping the telescope between the planet and the sky during the integration period. Celeste custom software tells the telescope secondary mirror when to chop and also keeps track of which position it is integrating on. The Moon was used as a flat-field reference for calibration since it was the only radiance source in the sky that completely filled the slit, was bright enough to register in short exposures and contained telluric absorption line information. We assume that at our small ~2 cm^{-1} spectral interval the Moon's thermal emission is essentially flat. We also selected maria regions near the limb and manually scanned over it during the integration to smooth out any intensity variations due to terrain differences.

The Celeste observations were obtained and reduced in the standard method whereby the spectra from two different nod positions are subtracted to remove any offset signal. In each of these nod positions the telescope chops between the sky and the planet, but the position of the planet is alternated to eliminate any possible biases either in the light path or electronic readout sequence. We refer to these as A (planet-sky) and B (sky-planet) nod positions. The response of the

array is then normalized by using the Moon flat-field. A total of 14 subtracted A-B pairs were combined to create the UKIRT spectrum shown in Figure 3 (green curve) which has an equivalent emission angle of 37°. This spectrum represents a total of 1 hour of integration time on the beacon region. A total of 44 subtracted A-B pairs were combined to create the IRTF spectrum shown in Figure 3 (blue curve), which has an equivalent emission angle of 44°. This spectrum represents a total of 2.35 hours of integration time on the beacon region. In both spectra the main C_2H_4 emission feature was shifted on the detector in the spatial direction to account for rotation of the planet, and also shifted spectrally to account for the change in radial velocity as the planet rotated. The CIRS data from two successive maps indicate that the beacon was moving at 2.6°/day (25.2 m/s, subsonic) in the summer of 2011 and 2.9°/day in the spring of 2012. The beacon was therefore centered near 57°W longitude on July 18, 2011 and 40°W longitude on April 2, 2012.

At UKIRT the intensity calibration for the Saturn spectrum was obtained by comparing it with a spectrum taken in a similar fashion (same instrument settings and procedure) on July 13, 2011 of the northern latitudes of Jupiter. For the Jupiter spectrum the slit length was also oriented east-west over latitude 59°N. These are auroral latitudes on the planet, but at the time of the observations there was no auroral activity registered at those longitudes (65° - 100° SIII). Auroral activity on Jupiter, when present, is usually strongly localized on a hot spot at ~180° SIII longitude. This was evident as there was no measurable ethylene emission observed on top of the continuum in the Jupiter spectrum. We proceeded to match the continuum intensity level of that spectrum to the continuum radiance provided by radiative transfer models according to the method outlined and used in Romani

et al. (2008). In this manner, the radiance uncertainty for the UKIRT Saturn spectrum is estimated at $\sim \pm 15\%$, mostly due to model emission angle uncertainties in the Jupiter spectrum. At the IRTF the intensity calibration for the Saturn spectrum was obtained using observations of Venus collected on the same day as the Saturn data, and also using the same procedure and similar instrument settings. The measured Venus spectrum was converted to real intensity units by using the Venera 15 average global spectrum (Zasova et al., 2004). The radiance uncertainty is estimated at $\sim \pm 10\%$, in this case mostly due to air mass extinction uncertainties at this wavelength and the absolute calibration of the Venera 15 spectrum.

Ethylene is detected as a band of lines at UKIRT in July 2011 but it is not present above the noise level in the IRTF data in April 2012. The Celeste data from the McMath-Pierce Telescope in May 2011 are presented in Figure 3 (red curve) as a comparison. The steps used in reducing, calibrating, and analyzing this spectrum were presented in Hesman et al. (2012). The equivalent emission angles of all three data sets are 35-43° which allows direct comparison of the calibrated intensity shown in Fig. 3. The strongest ethylene lines are evident with peaks at wavenumbers beyond 949.4 cm^{-1}, however the entire 2 cm^{-1} band pass is dominated by ethylene emission. The significantly increased emission between 948.5 and 949.4 cm^{-1} shown in the red curve (May 15, 2011) is not only the result of higher temperatures during this time period but also due to an increased amount of ethylene at pressures between 0.1 and 10 mbars on Saturn.

While the longitude extent of the ethylene emission region in the beacon (~20°) was larger than Celeste's single pixel field-of-view (2.6° longitude x 12.5° latitude) on UKIRT, the latitude extent was smaller. This was not the case in the Celeste spectra taken at the McMath-Pierce telescope in May 2011 (see Fig.1

of Hesman et al., 2012). When the ethylene lines became visible, the size of the beacon in the north/south direction in ethylene emission was larger than the McMath-Pierce beam. However, at UKIRT it was necessary to apply a correction for beam dilution in the latitude direction because the ethylene spot had reduced in size as shown by comparing Fig.1 of Hesman et al. (2012) to Fig. 2c. We detected ethylene emission in three Celeste pixels in the north/south direction, which corresponded to 12.5° in latitude at the beacon latitude. The actual extent of the ethylene emission was 6° as determined from the CIRS observations. Approximating both profiles as Gaussian, we adopted the ratio of these, 2.1, as the beam dilution factor. We estimate an uncertainty of 20% on this factor.

3. Data Analysis and Results

In this analysis the Saturn storm is broken into different time periods as presented in Fletcher et al. (2012). The time period before the storm erupted in December 2010 is referred to as the pre-storm in this discussion. The time period where two stratospheric beacons were present and growing in strength is referred to as storm phase 1 and lasted from January 2011 to May 2011. The merging of the two beacons to become one beacon, which produced the largest temperature difference from the pre-storm value of 140 K ever seen on Saturn, is referred to as storm phase 2 and lasted from May 2011 to August 2011. And finally, storm phase 3 was after the visible storm clouds dissipated in August 2011 but when infrared measurements were still showing changes from the pre-storm conditions in the stratosphere.

In order to retrieve ethylene abundances with time we first extract the temperatures inside the beacon over the pressure ranges where CIRS and Celeste are

sensitive. The temperature profiles are folded into the abundance retrievals which give a time series of ethylene abundances in the precursor period to the storm and the 3 time phases of the storm.

3.1. Temperatures in the Beacon

The temperature profile was retrieved using spectral bands separate from the ethylene region, in both the FP3 and FP4 focal planes. The same averaging used to produce the ethylene spectrum in the beacon region (as described in Section 2) was used to create the spectra used for temperature retrievals. Separate retrievals for upper tropospheric and stratospheric temperatures are performed using the constrained linear inversion algorithm described by Conrath et al. (1998). For the tropospheric retrievals, the spectral ranges from 600-620 and 640-660 cm^{-1} (FP3) are used where the atmospheric opacity is from the collision-induced S(1) line of hydrogen, assuming equilibrium hydrogen. Opacity from H_2-H_2, H_2-He, H_2-CH_4 pairs is included, using algorithms from Borysow et al. (1985, 1988) and Borysow and Frommhold (1986). A He/H_2 ratio of 0.135 is assumed (Conrath and Gautier, 2000) along with a pressure dependent CH_4 mole fraction profile based on the photochemical profile in Moses et al. (2000) scaled to a tropospheric value of of $4.5x10^{-3}$ as given in Flasar et al. (2005). The stratospheric temperatures are retrieved using the ν_4 band of CH_4 between 1250 and 1311 cm^{-1} (FP4). Methane transmittances were calculated using the correlated-k method (Lacis and Oinas, 1991), using line data from the GEISA 2003 line atlas (Jacquinet-Husson et al., 2005) with H_2/He broadening (Linda Brown, private communication).

We used the ν_4 band of CH_4 centered near 1304 cm^{-1} to derive the stratospheric temperature profile on Saturn for all of our spectral averages. In Figure 4a we show a comparison of CIRS spectra of Saturn prior to the storm, a spectrum

of a Saturn beacon acquired on January 14, 2012 and a spectrum of Jupiter's northern aurora acquired on January 13, 2001 during Cassini's flyby of the giant planet. The spectral resolution is 0.5 cm^{-1} and the emission angle is 67° for both Saturn spectra and 70° for the Jupiter spectrum. We selected three CH_4 features that sound different altitudes in the stratosphere. All are optically thick at the spectral resolution of CIRS. As described previously, the temperature inversion algorithm uses the entire ν_4 band but it is instructive to examine how these three spectral features constrain the temperature profile. In Figure 4b we show the retrieved temperature profiles for Saturn in September 2010 and in a beacon in January 2012 along with contribution functions for the three spectral features. The strongest CH_4 line at 1305.75 cm^{-1} sounds the 0.5 mbar level with half-power points near 0.1 and 1 mbar. The medium-strength feature at 1302.5 cm^{-1} sounds the 2 mbar level, and the weakest feature at 1310 cm^{-1} sounds the 5 mbar level. We therefore have sufficient vertical resolution to distinguish between different heating mechanisms for the beacon. Prior to the storm, the spectrum was nearly flat between 1304 and 1306 cm^{-1} (Fig. 4a, blue curve). This is the signature of a nearly isothermal profile for $p < 2$ mbar. The spectrum of a jovian aurora increases sharply from 1304 to 1306 cm^{-1} (Fig. 4a, red-dash curve) due to a heated layer at high altitudes around 1x10−3 mbar on Jupiter (Drossart et al., 1993). The spectrum of a Saturn beacon exhibits the opposite behavior. The strong CH_4 feature at 1305.75 cm^{-1} is observed to be in absorption (Fig. 4a, red curve). This is the result of a cold layer at 0.5 mbar residing above a hot layer at 2 mbar in the beacon. This is inconsistent with a high-altitude energy source, such as auroral heating. It is consistent with adiabatic heating in the downward phase of a gravity wave, as discussed by Hesman et al. (2012) and Fletcher et al. (2012).

Our temperature retrievals permit us to explore gradients in the profile of minor constituents over the 0.5 to 5 mbar range in Saturn's stratosphere where we have reliable temperatures. Figure 4b shows the temperature profile (solid red curve) retrieved from the beacon region in Saturn's northern storm region. The uncertainty limits in the retrieved temperature profile are approximately 1 K over the 0.1 to 10 mbar range in the stratosphere and over the 100 to 300 mbar range in the troposphere. Between these pressure regions, the inversion algorithm smoothly interpolates temperatures. The temperature profile is not well-determined at pressures less than 0.1 mbar. The retrieved temperatures for the CIRS data given in Table 1 are shown in Fig. 5.

The temperature profile used to interpret the Celeste C_2H_4 data was acquired 1-week later using the CIRS MIRMAP on July 26, 2011 (DOY = 207). The spatial extent of the Celeste slit was used to define the latitude range over which the CIRS temperature retrievals were performed. This retrieved temperature profile is shown as the green curve in Fig. 5. Fig. 5 illustrates that beacon temperatures in July 2011 remained stable at ~190 K at 1.3 mbar. The UKIRT observations were timed to be adjacent to CIRS observations so that CIRS data could be used to retrieve temperature.

3.2. Abundance Retrievals

The C_2H_4 abundance profile retrievals were performed using the Non-Linear Optimal Estimator for Multivariate Spectral Analysis (NEMESIS) code as described in Irwin et al. (2008). Absorption of the contributing species was calculated using the correlated-k method (Lacis and Oinas, 1991). The k-tables for C_2H_4 were calculated using line parameters based on data from the GEISA 2003 line atlas (Jacquinet-Husson et al., 2005) with modifications to the temperature ex-

ponent (set to 0.73), which is used in the relation of the temperature dependence of the pressure broadening coefficient, modified to use H_2 pressure broadening rather than N_2 (Bruno Bézard, private communication). Inputs into the model were the temperature profiles and an assumed ethylene mole fraction profile. A one-dimensional photochemical model was used along with a temperature profile of the beacon region to generate an ethylene mole fraction profile. The model takes into account the photolysis and chemical reactions that interlink the hydrocarbons with each other and atomic hydrogen. It solves their coupled continuity equations assuming steady state conditions. The net flux of the species includes terms for both transport (eddy mixing) and molecular diffusion. For a more detailed model description of the model see Romani et al. (2008). Ethylene has a photochemical lifetime of about 20 days in the 2 to 0.2 mbar region. The photochemical model predicts C_2H_4 abundance profiles for the warmest (~200 K) regions of Saturn's stratosphere that are enhanced by a factor of 2 in the 2 to 0.2 mbar altitude range over the ethylene abundances calculated for the unperturbed (140 K) atmosphere.

The CIRS C_2H_4 observations were obtained using nadir rather than limb data. Limb data is very scarce and do not cover the beacon. At 3.0 cm^{-1}, only one C_2H_4 emission feature is evident. At 0.5 cm^{-1} (CIRS) and at 0.1 cm^{-1} (Celeste) resolution, multiple emission lines of C_2H_4 of varying strength were detected. This gives us limited information about the vertical profile of C_2H_4. We used two different approaches to retrieve the abundance of C_2H_4. In the first approach, the theoretical ethylene photochemical profile was uniformly increased or decreased by a scaling factor to determine the best scale factor that reproduced the data. In the second, the scale factor applied to the theoretical ethylene photochemical profile was allowed to vary with altitude to produce a continuously-variable profile

that best fit the data. We call the first approach "scale factor" and the second "continuously-variable". Both techniques yield the same abundance at the peak of the contribution function near 2 mbar. In deciding which type of approach (scale factor or continuously-variable) to fit the data we looked at the contribution functions and at the goodness-of-fit of the model to the spectral lines.

In Fig. 6 three ethylene profiles are shown. The green curve shows the photochemical profile of ethylene which has been calculated using the photochemical model (Romani et al., 2008) using the temperature profile shown in black. The red curve is the profile that results when applying a single scale factor to the green curve in order to fit MIRMAP data taken in July 2011. The blue curve is a continuously-variable profile that was retrieved by letting the ethylene profile vary at each altitude from the photochemical profile. The contribution functions for these different abundance profiles is shown in Fig. 6. Fig. 7 shows the MIRMAP spectrum (black curve) and the models based on the two different retrieved abundance profiles shown in Fig. 6. As the residuals show, there is very little difference between the two model curves and both produce reduced χ^2, as reported by NEMESIS, indicating that they fit the data equally well. However, when moving to the 0.5 cm^{-1} data the situation changes. Fig. 8 shows the retrieved temperature profile for the COMPSIT data taken in January 2012 (black curve) and three ethylene abundance curves: the photochemical (green), the scale factor fit (red), and the continuously-variable retrieval (blue). In Fig. 9 the 0.5 cm^{-1} data is shown in black with the two models in red and blue. In this situation it is clear that the main ethylene feature at 949.5 cm^{-1}, as well as several nearby data points, is fit with greater accuracy using the continuously-variable profile, with the profile that scales the photochemical profile producing a much less desirable fit. In Figs. 10

and 11 the UKIRT data shows that both the scale factor and continuously-variable models fit within the error bars of the spectrum except near 950.0cm^{-1} where the continuously-variable profile is the only curve within the error bars. These tests of parameter space led us to use a continuously-variable profile approach to fitting the data at spectral resolutions higher than 2.5 cm^{-1}. We are not sensitive over a large altitude space as one is when doing limb studies but clearly the data at higher spectral resolution is allowing us to retrieve more information out of the analysis rather than just one scale factor.

Even though the differences in the retrieved spectra are small when comparing the scale factor to the continuously-variable approach, we preferred the continuously-variable approach for finer spectral resolutions (0.5 and 0.1 cm^{-1}). Essentially, the continuously-variable fit indicates at what altitude this species has the largest contribution. For these observations this corresponds to the 1.3 mbar pressure region and therefore all results are presented at the 1.3 mbar level. The profiles retrieved in a continuously-variable fashion are shown in Fig. 12. It is necessary to note that these profiles all peak at the 1.3 mbar pressure range except for the profile on March 3, 2011 (DOY = 062) which peaks at a slightly lower pressure level; this data set pertains to the time period before the two beacons merged. The 1.3 mbar abundances of ethylene with time are shown in Fig. 13.

4. Discussion

The detection of ethylene in the northern storm region is significant because it is a short-lived tracer of photochemistry in Saturn's stratosphere. CIRS measured detectable levels of C_2H_4 for approximately 10 months. However, in early 2012 ethylene emission faded more quickly than the temperature decreased in the

beacon region. Fig. 5 shows the retrieved temperature profiles for the different phases of the storm that are defined in Fig. 13. In the first phase of the storm there were two beacons and the peak temperatures occurred near the 0.5 mbar level (dash-dot, dotted curves; Fig. 5). In May 2011, the two beacons merged and the resulting beacon exhibited its maximum temperature of ~220 K and dropped in altitude to near the 2 mbar pressure level (solid curves). By August 2011 the radio signals that indicate lightning on Saturn fell off abruptly, thus marking the end of the active storm period in the troposphere resulting in the dissipation of the upper tropospheric storm clouds (Sayanagi et al., 2013). However, in the stratosphere the temperature of the beacon remained well above pre-storm levels. Over the next two years (storm phase 3) the surviving beacon continued to cool until it was no longer detectable by early 2014.

Although both the ethylene abundance and the atmospheric temperature were enhanced in the beacon region(s), the two phenomena followed different chronologies. Ethylene was detectable for approximately 10 months, from 150 to 425 days after the start of the storm, whereas enhanced temperatures in the beacon region were observed for nearly 3 years. In particular, C_2H_4 emission faded quickly in early 2012. Between January 2012 (burgundy and green solid curves Fig. 12) and April 2012 (red-dashed curve Fig 12) the ethylene emission dropped below our detectable limit. However, in April 2012 the temperature at 2 mbar was still 180 K (red-dashed curve Fig 5), well above the pre-storm temperature. Thus, it appears that ethylene became detectable once the temperatures rose above about ~180 K, and faded quickly once the temperatures fell below ~180 K, whereas the temperature anomaly decayed over a time period of about 3 years. Therefore, the changes in ethylene abundance occurred on a shorter timescale than the cooling

of the stratospheric temperatures in the beacon. The persistence of the ethylene enhancement for ~10 months is longer than the calculated photochemical lifetime of ~20-30 days. However, it should be noted that the calculated ethylene lifetime applies to nominal, rather than enhanced abundances of C_2H_4. One possible scenario is that with the higher temperatures the C_2H_4 photochemical system shifted to a new equilibrium state in which the ethylene abundance was maintained at the enhanced values until the temperature dropped below a certain threshold. The rapid disappearance of C_2H_4 in early 2012 is consistent with the ~ 20-30 day lifetime.

We now examine whether the greatly enhanced ethylene emission could possibly be due to only enhanced hydrocarbon production at pressures less than 0.01 mbar in the region of its photochemical production from CH_4 photolysis. CIRS data alone do not rule out this mechanism because they are not sensitive to C_2H_4 at pressures less than 0.01 mbar. However, when combined with Celeste observations (as shown in Fig. 14) it is possible to assess if microbar enhancement of ethylene can be the sole cause for enhanced ethylene emission in the beacon region. In Fig. 14 a synthetic spectrum is calculated for a C_2H_4 profile that is enhanced by a factor of 100 over the photochemical profile only at pressure levels less than 0.01 mbar (microbar region). Increasing the ethylene in the upper stratosphere by such a large factor does not fit the Celeste data as shown by the red dashed curve in Fig. 14a. There is a severe lack of ethylene emission in the strongest feature at 949.4 cm^{-1} as well as in the wings as compared with the UKIRT spectrum. The Celeste data also constrain the minimal detectable abundance of C_2H_4. The synthetic spectrum calculated using the photochemical profile (blue curve) shows that even with the heightened temperatures of the beacon

the photochemical profile produces ethylene emission below our detection limit. The Celeste data can therefore be used to set limits on the altitude over which the ethylene enhancement is present when used in conjunction with the CIRS observations. It is only when the amount of ethylene at pressures greater than 0.01 mbar is increased above the photochemical that the Celeste spectrum is able to be fit. Therefore even if the production rate at the microbar level was greatly increased it is not possible to produce the observed Celeste spectra with only an adjustment made in the microbe region. However, because this work shows that the abundance of C_2H_4 at the millibar-level is enhanced over the pre-storm value measured by UVIS (Shemansky and Liu, 2012) and it stays enhanced for a significant time period there must be a mechanism altering ethylene at the millibar level, as opposed to the microbar level.

Ethylene is an important species on Saturn because it has photochemical pathways that connect together C_2H_2 and C_2H_6 that have a long observational history (e.g. Sada et al., 2005). In Hesman et al. (2012) we examined the effect of the elevated temperature in the beacon region on the gas phase photochemistry of ethylene. We found that with nominal gas phase photochemistry the photochemical model produced only a doubling in the ethylene volume mixing ratios due to the temperature increase alone whereas our observations indicate a 100-fold increase in the ethylene abundance at the 2 mbar altitude region. In the region of the observed enhanced ethylene emission (0.1 mbar<p<10 mbar) the principal source of C_2H_4 comes from reactions involving C_2H_3, the vinyl radical:

$$C_2H_3 + H_2 \rightarrow C_2H_4 + H \quad \text{(R1)}$$

$$C_2H_3 + H + M \rightarrow C_2H_4 + M \quad \text{(R2)}$$

where M is any other atmospheric molecule. The primary source of the vinyl

radical is acetylene. Ethylene's primary sink is:

$$C_2H_4 + H + M \rightarrow C_2H_5 + M \quad \text{(R3)}$$

with photolysis playing a lesser role:

$$C_2H_4 + h\nu \rightarrow C_2H_2 + H_2 \quad \text{(R4)}$$

$$C_2H_4 + h\nu \rightarrow C_2H_2 + 2H \quad \text{(R5)}$$

In this region ethylene is in photochemical equilibrium with production and loss balancing each other with a per molecule lifetime on the order of 20 days. As noted in Hesman et al. (2012) there could be either an unknown source of ethylene that turns on and then off with the rising and then falling temperatures in the beacon region, or a suppression of the major sink of ethylene, R3.

In order to investigate these processes, we examined the effects of not only the elevated temperature on the nominal gas phase photochemistry, but also the effects of the enhanced abundances retrieved from the observations. We calculated the photolysis rates, chemical reaction rates and free radical mixing ratios in the beacon region with the gas phase photochemical model mixing ratios artificially enhanced to match the retrieved values in the region between 10 and 0.1 mbar. With these elevated abundances, ethylene becomes a significant absorber in part of the UV spectrum where the hydrocarbons absorb and the overall ethylene photolysis rate in the atmospheric region increases by a factor of ~20. This could explain in part the persistent ethylene enhancement during the storm as C_2H_4 photolysis leads to C_2H_2 production, which leads to C_2H_3 production and finally back to C_2H_4 (R1 & R2). This is in contrast to R3 where C_2H_5 production leads to CH_3 production and eventually to either CH_4 or C_2H_6. However, this does not explain the initial ethylene enhancement or its decay back to pre-storm

values because with the elevated temperature, the gas kinetic reaction rate for R3 increases and the overall reaction remains the dominant sink for ethylene. With elevated temperatures only 36% of ethylene loss is via photolysis and 64% is via R3, whereas with elevated temperatures and enhanced mixing ratios, photolysis is only 15% of the total ethylene loss rate while R3 is 85% of the loss rate. Thus R3 increases more in relative importance than the photolysis sink. However, this loss via H is probably unsustainable since in the 10 to 0.1 mbar region the H atom loss rate is $\sim$ 3x the production rate with 86% of the loss rate coming from the reaction with ethylene.

A possibility in the beacon region is a "turning-on" of a photochemical sink for H atoms. In this case, the suppressed H atom abundance would consequently result in the C_2H_4 mixing ratio increasing. The enhanced ethylene mixing ratios would shift towards a new photochemical equilibrium and the ethylene enhancement would persist until the temperatures cooled to a point where the H atom sink "turns-off". The return of the H atom abundance to pre-storm levels would then reduce the ethylene mixing ratio to its nominal profile. For this H atom sink to compete with R3 its overall reaction rate must be roughly equivalent to R3. The overall reaction rate for R3 is $k_{R3} * [H] * [C_2H_4] * [M]$ where the square brackets denote the number density and M is any other atmospheric molecule. Our kinetic rate constant for R3, k_{R3}, uses the following values from the review by Baulch et al. (1995):

$$k_{R3} = (k_0 k_\infty M)/(k_0 M + k_\infty) \quad (1)$$

$$k_0 = 1.3\text{x}10^{-29} e^{-380.0/T} \quad (2)$$

$$k_\infty = 6.6\text{x}10^{-15} T^{1.28} e^{-650.0/T} \quad (3)$$

where k_0 is the kinetic rate constant at low pressure and k_∞ is the kinetic rate constant at high pressure. Similarly, it could be reasoned that any ethylene source not present in the model would need an overall reaction rate greater than or equal to R3 to be able to compete with the R3 sink for C_2H_4.

Gas phase chemistry alone may be insufficient to explain the observed ethylene enhancement on Saturn. We therefore consider other pathways for producing ethylene. One possibility is that the ethylene enhancement is due to heterogeneous chemistry involving Saturn's stratospheric haze (West et al., 2009). We assume that the haze is primarily composed of hydrocarbons as a result of gas phase methane photolysis and subsequent photochemistry producing higher order hydrocarbons. The haze can work either as a direct source of C_2H_4, as an indirect source, or catalytically. The first instance would involve the haze warming in response to the rising atmospheric temperatures in the beacon thereby evaporating ethylene ice which would lead to increasing ethylene in the vapor phase. This is an unlikely scenario because under nominal conditions C_2H_4 does not condense in Saturn's stratosphere. As an indirect source there are several possible mechanisms. One way is that while the warm stratospheric haze is in the solid state chemical reactions could convert its hydrocarbon component to C_2H_4 which then vaporizes. Another way is that the haze could vaporize and release complex hydrocarbons (such as polyacetylene) that undergo gas phase photochemistry to produce ethylene. In either case, the hydrocarbon component of the stratospheric haze would have to be known (or modeled) and a complex chemical system (solid state and/or gas phase) would have to be modeled. Finally, the ethylene enhancement could result due to a catalytic source whereby the warm haze acts as a catalyst that either forms C_2H_4 from other gas phase hydrocarbons or acts as a catalytic

sink for H atoms. Either mechanism would result in an enhancement of the ethylene mixing ratio. However, these mechanisms require theoretical study to see if they can be reproduced based on the results found here.

5. Conclusions

Eleven CIRS data sets and two ground-based (UKIRT and IRTF) data sets were studied in this analysis of ethylene emission throughout the northern storm time period. It has been deduced that ethylene emission appears to "turn-on" when temperatures in the beacon increased above 180 K and ceased when temperatures fell back below that threshold. During this time period the ethylene emission varied between 20 and 100 ppb at 1.3 mbars. From these findings it was shown that there must be a mechanism altering ethylene at the millibar level rather than the microbar level where it is produced. Gas phase chemistry may be insufficient to explain the enhanced ethylene abundances and other sources such as heterogeneous chemistry involving Saturn's stratospheric haze may need to be considered. These mechanisms require further investigation, but the results presented here can provide the framework for this work.

Acknowledgments

The authors want to thank the Cassini/CIRS calibration team for their assistance in the calibration of these data sets. The authors also wish to thank the United Kingdom Infrared Telescope staff and the NASA Infrared Telescope staff for their assistance during these observations. This research was supported by the NASA Cassini/CIRS project, by the NASA Planetary Astronomy (PAST) Program grant number NNX11AJ47G, and the NASA Cassini Data Analysis Par-

599 ticipating Scientists (CDAPS) Program grant number NNX12AC24G. Fletcher is
600 supported by a Royal Society Research Fellowship at the University of Oxford.

601 References

602 Baulch, D. L., Cobos, C. J., Cox, R. A., Frank, P., Hayman, G., Just, T., Kerr, J. A.,
603 Murrells, T., Pilling, M. A., Troe, J., Walker, R. W., Warnatz, J., 1995. Eval-
604 uated kinetic data for combustion modelling supplement I. Journal of Physics
605 Conference Series 23, 847–1033.

606 Beebe, R. F., Barnet, C., Sada, P. V., Murrell, A. S., 1992. The onset and growth
607 of the 1990 equatorial disturbance on Saturn. Icarus 95, 163–172.

608 Bézard, B., Moses, J. I., Lacy, J., Greathouse, T., Richter, M., Griffith, C., 2001.
609 Detection of Ethylene (C_2H_4) on Jupiter and Saturn in Non–Auroral Regions.
610 In: AAS/Division for Planetary Sciences Meeting Abstracts #33. Vol. 33 of
611 Bulletin of the American Astronomical Society. p. 1079.

612 Borysow, A., Frommhold, L., 1986. Theoretical collision-induced rototransla-
613 tional absorption spectra for the outer planets - H_2-CH_4 pairs. ApJ 304, 849–
614 865.

615 Borysow, J., Frommhold, L., Birnbaum, G., 1988. Collison-induced rototransla-
616 tional absorption spectra of H_2-He pairs at temperatures from 40 to 3000 K.
617 ApJ 326, 509–515.

618 Borysow, J., Trafton, L., Frommhold, L., Birnbaum, G., 1985. Modeling of
619 pressure-induced far-infrared absorption spectra of molecular hydrogen pairs.
620 ApJ 296, 644–654.

Conrath, B. J., Gautier, D., 2000. Saturn Helium Abundance: A Reanalysis of Voyager Measurements. Icarus 144, 124–134.

Conrath, B. J., Gierasch, P. J., Ustinov, E. A., 1998. Thermal Structure and Para Hydrogen Fraction on the Outer Planets from Voyager IRIS Measurements. Icarus 135, 501–517.

Drossart, P., Bezard, B., Atreya, S. K., Bishop, J., Waite, Jr., J. H., Boice, D., 1993. Thermal profiles in the auroral regions of Jupiter. J. Geophys. Res. 98, 18803.

Dyudina, U. A., Ingersoll, A. P., Ewald, S. P., Porco, C. C., Fischer, G., Kurth, W. S., West, R. A., 2010. Detection of visible lightning on Saturn. Geophys. Res. Lett. 37, L09205.

Encrenaz, T., Combes, M., Zeau, Y., Vapillon, L., Berezne, J., 1975. A tentative identification of C_2H_4 in the spectrum of Saturn. A&A 42, 355–356.

Fischer, G., Kurth, W. S., Gurnett, D. A., Zarka, P., Dyudina, U. A., Ingersoll, A. P., Ewald, S. P., Porco, C. C., Wesley, A., Go, C., Delcroix, M., 2011. A giant thunderstorm on Saturn. Nature 475, 75–77.

Flasar, F. M., Achterberg, R. K., Conrath, B. J., Pearl, J. C., Bjoraker, G. L., Jennings, D. E., Romani, P. N., Simon-Miller, A. A., Kunde, V. G., Nixon, C. A., Bézard, B., Orton, G. S., Spilker, L. J., Spencer, J. R., Irwin, P. G. J., Teanby, N. A., Owen, T. C., Brasunas, J., Segura, M. E., Carlson, R. C., Mamoutkine, A., Gierasch, P. J., Schinder, P. J., Showalter, M. R., Ferrari, C., Barucci, A., Courtin, R., Coustenis, A., Fouchet, T., Gautier, D., Lellouch, E., Marten, A., Prangé, R., Strobel, D. F., Calcutt, S. B., Read, P. L., Taylor, F. W., Bowles, N.,

644 Samuelson, R. E., Abbas, M. M., Raulin, F., Ade, P., Edgington, S., Pilorz, S.,
645 Wallis, B., Wishnow, E. H., 2005. Temperatures, Winds, and Composition in
646 the Saturnian System. Science 307, 1247–1251.

647 Fletcher, L. N., Hesman, B. E., Achterberg, R. K., Irwin, P. G. J., Bjoraker, G.,
648 Gorius, N., Hurley, J., Sinclair, J., Orton, G. S., Legarreta, J., García-Melendo,
649 E., Sánchez-Lavega, A., Read, P. L., Simon-Miller, A. A., Flasar, F. M., 2012.
650 The origin and evolution of Saturn's 2011-2012 stratospheric vortex. Icarus
651 221, 560–586.

652 Fletcher, L. N., Hesman, B. E., Irwin, P. G. J., Baines, K. H., Momary, T. W.,
653 Sanchez-Lavega, A., Flasar, F. M., Read, P. L., Orton, G. S., Simon-Miller,
654 A. A., Hueso, R., Bjoraker, G. L., Mamoutkine, A., del Rio-Gaztelurrutia, T.,
655 Gomez, J. M., Buratti, B., Clark, R. N., Nicholson, P. D., Sotin, C., 2011.
656 Thermal Structure and Dynamics of Saturn's Northern Springtime Disturbance.
657 Science 332, 1413–1417.

658 Hesman, B. E., Bjoraker, G. L., Sada, P. V., Achterberg, R. K., Jennings, D. E.,
659 Romani, P. N., Lunsford, A. W., Fletcher, L. N., Boyle, R. J., Simon-Miller,
660 A. A., Nixon, C. A., Irwin, P. G. J., 2012. Elusive Ethylene Detected in Saturn's
661 Northern Storm Region. ApJ 760, 24.

662 Hesman, B. E., Jennings, D. E., Sada, P. V., Bjoraker, G. L., Achterberg, R. K.,
663 Simon-Miller, A. A., Anderson, C. M., Boyle, R. J., Nixon, C. A., Fletcher,
664 L. N., McCabe, G. H., 2009. Saturn's latitudinal C_2H_2 and C_2H_6 abundance
665 profiles from Cassini/CIRS and ground-based observations. Icarus 202, 249–
666 259.

667 Hueso, R., Sánchez-Lavega, A., 2004. A three-dimensional model of moist con-
668 vection for the giant planets II: Saturn's water and ammonia moist convective
669 storms. Icarus 172, 255–271.

670 Irwin, P. G. J., Teanby, N. A., de Kok, R., Fletcher, L. N., Howett, C. J. A.,
671 Tsang, C. C. C., Wilson, C. F., Calcutt, S. B., Nixon, C. A., Parrish, P. D.,
672 2008. The NEMESIS planetary atmosphere radiative transfer and retrieval tool.
673 J. Quant. Spec. Radiat. Transf. 109, 1136–1150.

674 Jacquinet-Husson, N., Scott, N. A., Chedin, A., Garceran, K., Armante, R.,
675 Chursin, A. A., Barbe, A., Birk, M., Brown, L. R., Camy-Peyret, C., Claveau,
676 C., Clerbaux, C., Coheur, P. F., Dana, V., Daumont, L., Debacker-Barilly, M. R.,
677 Flaud, J. M., Goldman, A., Hamdouni, A., Hess, M., Jacquemart, D., Kopke, P.,
678 Mandin, J. Y., Massie, S., Mikhailenko, S., Nemtchinov, V., Nikitin, A., Newn-
679 ham, D., Perrin, A., Perevalov, V. I., Regalia-Jarlot, L., Rublev, A., Schreier,
680 F., Schult, I., Smith, K. M., Tashkun, S. A., Teffo, J. L., Toth, R. A., Tyuterev,
681 V. G., Vander Auwera, J., Varanasi, P., Wagner, G., 2005. The 2003 edition of
682 the GEISA/IASI spectroscopic database. Journal of Quantitative Spectroscopy
683 and Radiative Transfer 95, 429–467.

684 Jennings, D. E., Romani, P. N., Bjoraker, G. L., Sada, P. V., Nixon, C. A.,
685 Lunsford, A. W., Boyle, R. J., Hesman, B. E., McCabe, G. H., 2009. 12C/13C
686 Ratio in Ethane on Titan and Implications for Methane's Replenishment. Jour-
687 nal of Physical Chemistry A 113, 11101–11106.

688 Lacis, A. A., Oinas, V., 1991. A description of the correlated-k distribution
689 method for modelling nongray gaseous absorption, thermal emission, and mul-

690 tiple scattering in vertically inhomogeneous atmospheres. J. Geophys. Res. 96,
691 9027–9064.

692 Moses, J. I., Bézard, B., Lellouch, E., Gladstone, G. R., Feuchtgruber, H., Allen,
693 M., 2000. Photochemistry of Saturn's Atmosphere. I. Hydrocarbon Chemistry
694 and Comparisons with ISO Observations. Icarus 143, 244–298.

695 Romani, P. N., Jennings, D. E., Bjoraker, G. L., Sada, P. V., McCabe, G. H.,
696 Boyle, R. J., 2008. Temporally varying ethylene emission on Jupiter. Icarus
697 198, 420–434.

698 Sada, P. V., Bjoraker, G. L., Jennings, D. E., Romani, P. N., McCabe, G. H.,
699 2005. Observations of C_2H_6 and C_2H_2 in the stratosphere of Saturn. Icarus 173,
700 499–507.

701 Sanchez-Lavega, A., Colas, F., Lecacheux, J., Laques, P., Parker, D., Miyazaki, I.,
702 1991. The Great White Spot and disturbances in Saturn's equatorial atmosphere
703 during 1990. Nature 353, 397–401.

704 Sánchez-Lavega, A., del Río-Gaztelurrutia, T., Delcroix, M., Legarreta, J. J.,
705 Gómez-Forrellad, J. M., Hueso, R., García-Melendo, E., Pérez-Hoyos, S.,
706 Barrado-Navascués, D., Lillo, J., International Outer Planet Watch Team
707 IOPW-PVOL, 2012. Ground-based observations of the long-term evolution and
708 death of Saturn's 2010 Great White Spot. Icarus 220, 561–576.

709 Sánchez-Lavega, A., del Río-Gaztelurrutia, T., Hueso, R., Gómez-Forrellad,
710 J. M., Sanz-Requena, J. F., Legarreta, J., García-Melendo, E., Colas, F.,
711 Lecacheux, J., Fletcher, L. N., Barrado y Navascués, D., Parker, D., Interna-
712 tional Outer Planet Watch Team, Akutsu, T., Barry, T., Beltran, J., Buda, S.,

Combs, B., Carvalho, F., Casquinha, P., Delcroix, M., Ghomizadeh, S., Go, C., Hotershall, J., Ikemura, T., Jolly, G., Kazemoto, A., Kumamori, T., Lecompte, M., Maxson, P., Melillo, F. J., Milika, D. P., Morales, E., Peach, D., Phillips, J., Poupeau, J. J., Sussenbach, J., Walker, G., Walker, S., Tranter, T., Wesley, A., Wilson, T., Yunoki, K., 2011. Deep winds beneath Saturn's upper clouds from a seasonal long-lived planetary-scale storm. Nature 475, 71–74.

Sayanagi, K. M., Dyudina, U. A., Ewald, S. P., Fischer, G., Ingersoll, A. P., Kurth, W. S., Muro, G. D., Porco, C. C., West, R. A., 2013. Dynamics of Saturn's great storm of 2010-2011 from Cassini ISS and RPWS. Icarus 223, 460–478.

Shemansky, D., Liu, X., 2012. Saturn upper atmospheric structure from Cassini EUV and FUV occultations. Can. J. Phys. Hunten special issue 90, 817–831.

Sromovsky, L. A., Baines, K. H., Fry, P. M., 2013. Saturn's Great Storm of 2010-2011: Evidence for ammonia and water ices from analysis of VIMS spectra. Icarus , 402–418.

West, R. A., Baines, K. H., Karkoschka, E., Sánchez-Lavega, A., 2009. Clouds and Aerosols in Saturn's Atmosphere. In: Dougherty, M. K., Esposito, L. W., & Krimigis, S. M. (Ed.), Saturn from Cassini-Huygens. pp. 161–179.

Zasova, L. V., Moroz, V. I., Formisano, V., Ignatiev, N. I., Khatuntsev, I. V., 2004. Infrared spectrometry of Venus: IR Fourier spectrometer on Venera 15 as a precursor of PFS for Venus express. Advances in Space Research 34, 1655–1667.

Observation Name	**Day of Year**	**Date**	**Resolution** (cm^{-1})	**Average Latitude** (degrees)	**Average Longitude** (degrees)	**Average Emission Angle** (degrees)	**Number of Spectra**
CIRS_137SA_COMPSIT004	254	11-Sep-10	0.53	37.5	164.7	72.9	4473
CIRS_145SA_COMPSIT007 (Beacon 2)	62	3-Mar-11	0.53	26.8	263.0	66.5	170
CIRS_145SA_COMPSIT007 (Beacon 1)	62	3-Mar-11	0.53	34.1	109.0	76.0	170
CIRS_146SA_COMPSIT003 (Beacon 2)	71	12-Mar-11	0.53	32.1	267.8	45.9	84
CIRS_146SA_COMPSIT004 & COMPSIT005 (Beacon 1)	72, 73	13/14-Mar-11	0.53	35.2	159.2	50.0	392
CIRS_148SA_MIRMAP001	124	4-May-11	2.50	37.6	289.1	38.0	304
CIRS_150SA_COMPSIT001	188	7-Jul-11	0.53	38.6	30.9	40.2	129
CIRS_151SA_MIRMAP001	207	26-Jul-11	2.50	40.9	71.9	41.4	688
CIRS_158SA_MIRMAP001	337	3-Dec-11	2.50	37.8	66.0	38.4	708
CIRS_159SA_COMPSIT004	13	13-Jan-12	0.53	38.5	170.1	65.9	126
CIRS_159SA_COMPSIT005	14	14-Jan-12	0.53	33.3	173.9	72.8	126
CIRS_161SA_COMPSIT001	47	16-Feb-12	0.53	33.8	269.1	68.7	129
CIRS_164SA_COMPSIT002	107	16-Apr-12	0.53	38.7	86.0	71.2	128

Table 1: Cassini CIRS observations of the beacon(s) throughout 2011 and 2012. The first entry is a pre-storm spectrum from 2010 that is used for comparison against the storm spectra. The observations in March 2011 are before the beacons merged. In these observations both Beacon 1 and 2 have been analyzed separately to look for signatures of ethylene.

Observation Name	**Average Latitude** (degrees)	**Ethylene Detected?**	**Retrieved Scale Factor**	**1.3mbar VMR** (ppb)
CIRS_137SA_COMPSIT004	37.5	no	< 35	
CIRS_145SA_COMPSIT007 (Beacon 2)	26.8	no	< 70	
CIRS_145SA_COMPSIT007 (Beacon 1)	34.1	marginal	23 ± 3	8 ± 3
CIRS_146SA_COMPSIT003 (Beacon 2)	32.1	no	< 150	
CIRS_146SA_COMPSIT004 & COMPSIT005 (Beacon 1)	35.2	no	< 30	
CIRS_148SA_MIRMAP001	37.6	yes	70± 3	92 ± 6
CIRS_150SA_COMPSIT001	38.6	yes	76 ± 12	51 ± 16
CIRS_151SA_MIRMAP001	40.9	yes	113 ± 7	92 ± 8
CIRS_158SA_MIRMAP001	37.8	yes	72 ± 7	59 ± 6
CIRS_159SA_COMPSIT004	38.5	yes	67 ± 10	25 ± 9
CIRS_159SA_COMPSIT005	33.3	yes	114 ± 10	39 ± 13
CIRS_161SA_COMPSIT001	33.8	yes	74 ± 10	28 ± 9
CIRS_164SA_COMPSIT002	38.7	no	< 100	

Table 2: Cassini CIRS observations of the beacon(s) throughout 2011 and 2012. The first entry is a pre-storm spectrum from 2010 that is used for comparison against the storm spectra. The observations in March 2011 are before the beacons merged. In these observations both Beacon 1 and 2 have been analyzed separately to look for signatures of ethylene. This table provides the value required to scale the ethylene photochemical profile in order to fit the data.

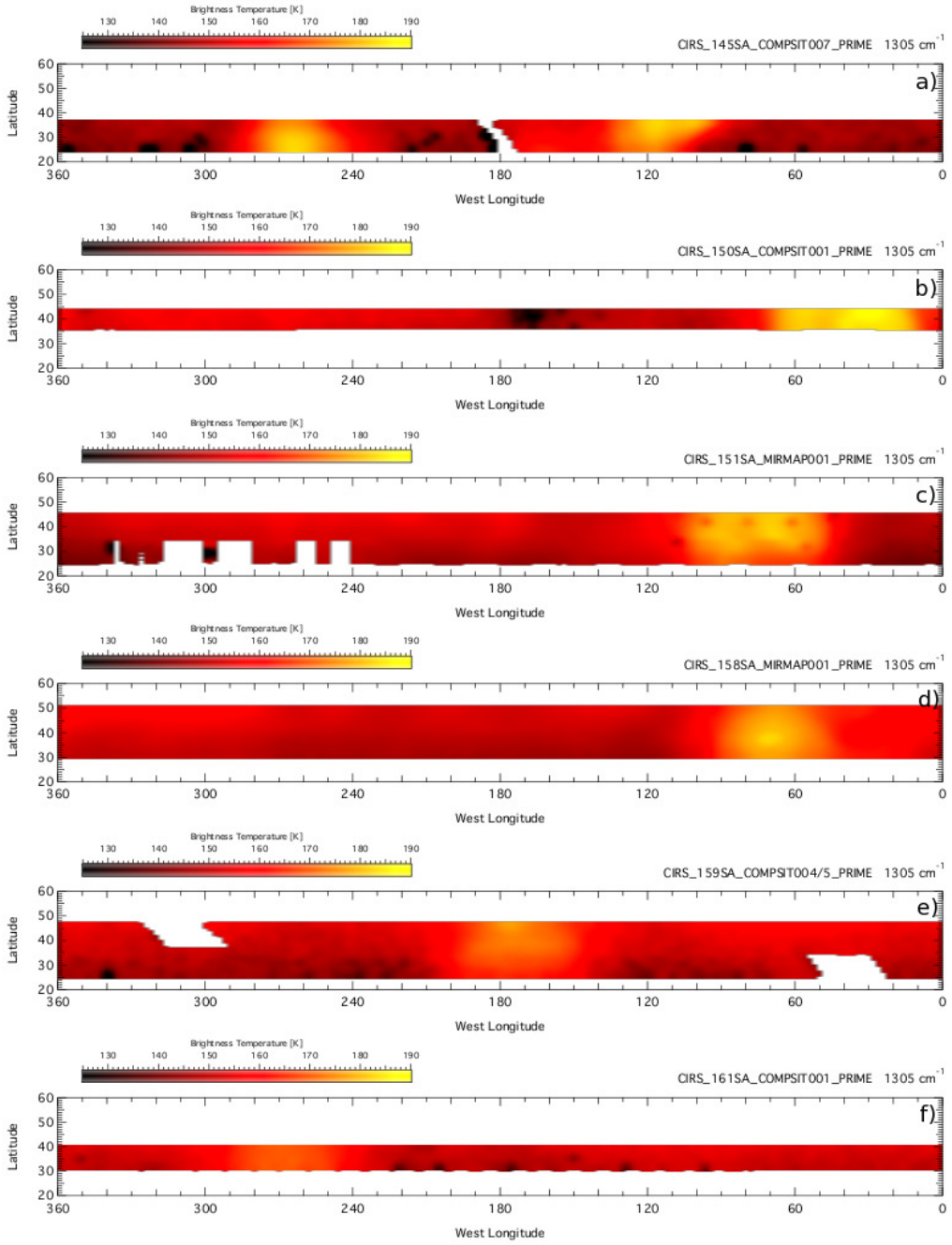

Figure 1: The 0.5 cm^{-1} (labeled COMPSIT) and 2.5 cm^{-1} (labeled MIRMAP) CIRS maps over the northern storm latitude for a) March 3, 2011, b) July 7, 2011, c) July 26, 2011, d) December 3, 2011, e) January 13-14, 2012, f) February 16, 2012. Left panel: These cylindrical maps shows the brightness temperature in the methane band at 1305 cm^{-1} for 5 spatial elements centered near the storm latitude. Longitudinal coverage was obtained for one rotation of Saturn. All maps have spatial resolutions of 2° by 2° and are given in planetographic coordinates.

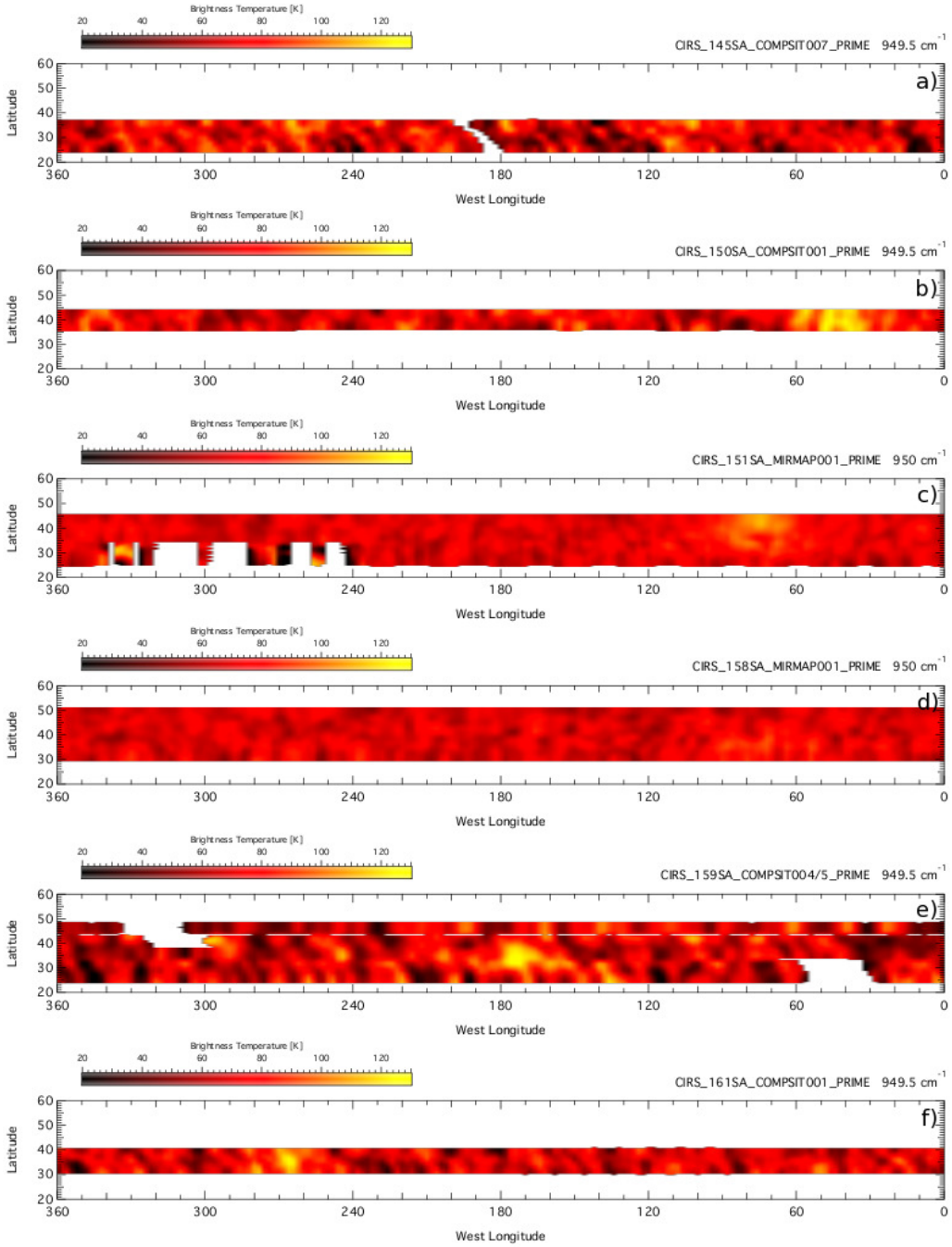

Figure 2: The 0.5 cm^{-1} (labeled COMPSIT) and 2.5 cm^{-1} (labeled MIRMAP) CIRS maps over the northern storm latitude for a) March 3, 2011, b) July 7, 2011, c) July 26, 2011, d) December 3, 2011, e) January 13-14, 2012, f) February 16, 2012. Left panel: These cylindrical maps shows the brightness temperature center of the ethylene band near 950 cm^{-1} for 5 spatial elements centered near the storm latitude. Longitudinal coverage was obtained for one rotation of Saturn. All maps have spatial resolutions of 2° by 2° and are given in planetographic coordinates.

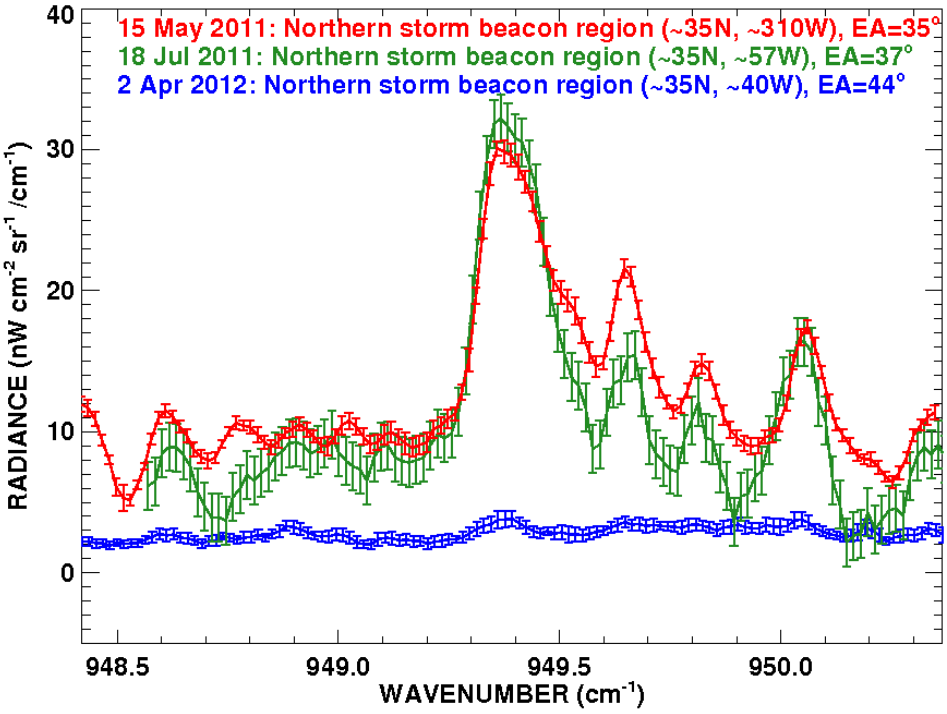

Figure 3: The 0.1 cm^{-1} Celeste spectra obtained from the McMath-Pierce Telescope on May 15, 2011 (red curve), the United Kingdom Infrared Telescope on July 18, 2011 (green curve), and the NASA Infrared Telescope Facility on April 2, 2012 (blue curve). The blue curve shows that by April 2012 ethylene emission in Saturn's beacon region has ceased. The analysis of the initial ethylene detection from McMath-Pierce is presented in Hesman et al. (2012).

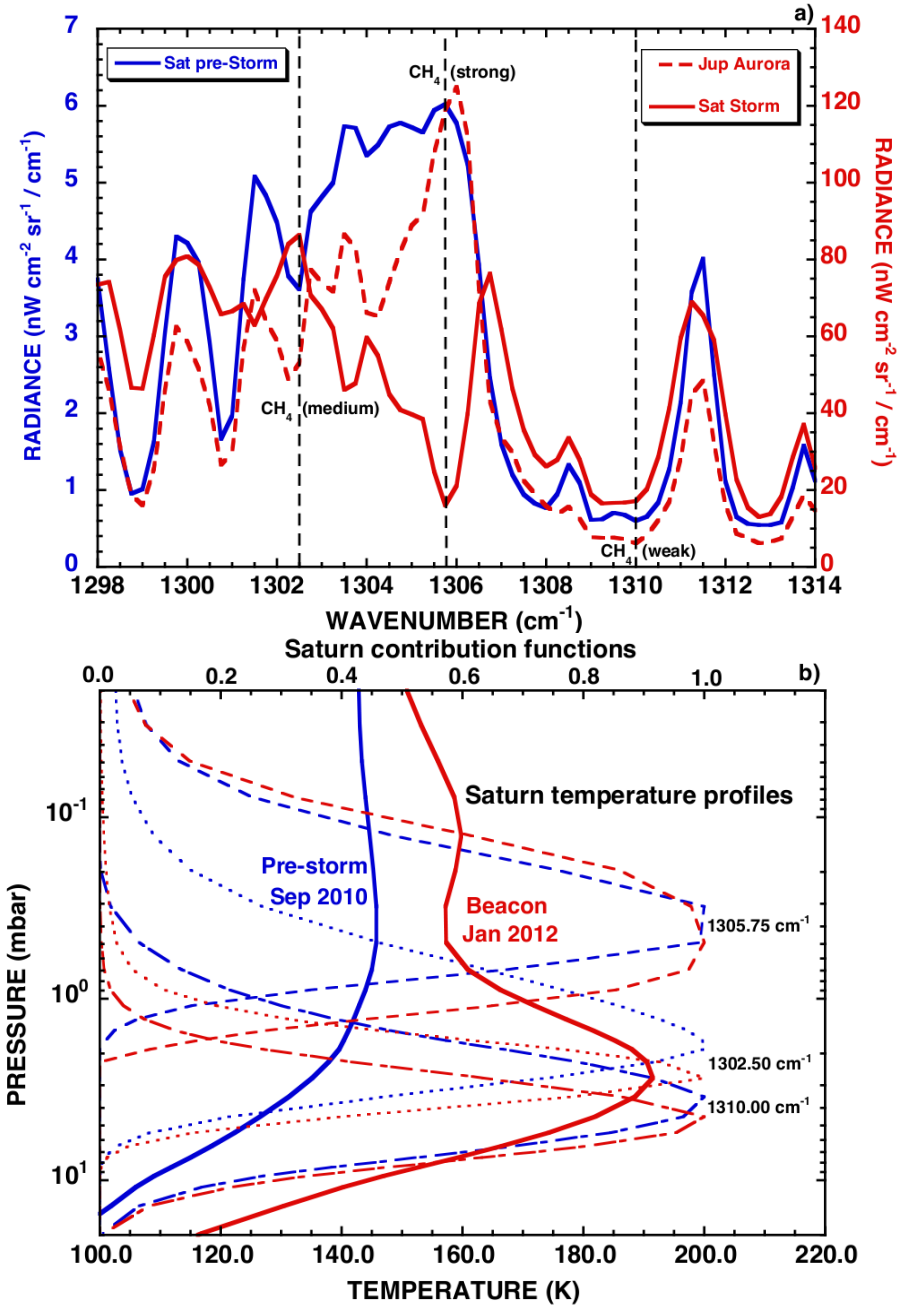

Figure 4: a) The 0.5 cm^{-1} CH_4 spectra of Saturn prior to the storm (blue curve), a spectrum of Saturn's beacon acquired on 2012 January 14 (red solid curve) and a spectrum of Jupiter's northern aurora acquired on 2001 Jan 13 (red dashed curve). The emission angles are 67° for both Saturn spectra and 70° for the Jupiter spectrum. b) The temperature profiles for the pre-storm conditions (blue curve) and the in beacon conditions (red curve). The contribution functions are shown for the weak (1310.0 cm^{-1}), medium (1302.50 cm^{-1}), and strong (1305.75 cm^{-1}) methane lines. The blue solid curve between 1304 -1306 cm^{-1} is practically flat indicating that the temperature is nearly isothermal (blue solid curve; panel b). The red solid curve between 1304 -1306 cm^{-1} shows absorption indicating a cold layer over a warm layer (red solid curve; panel b).

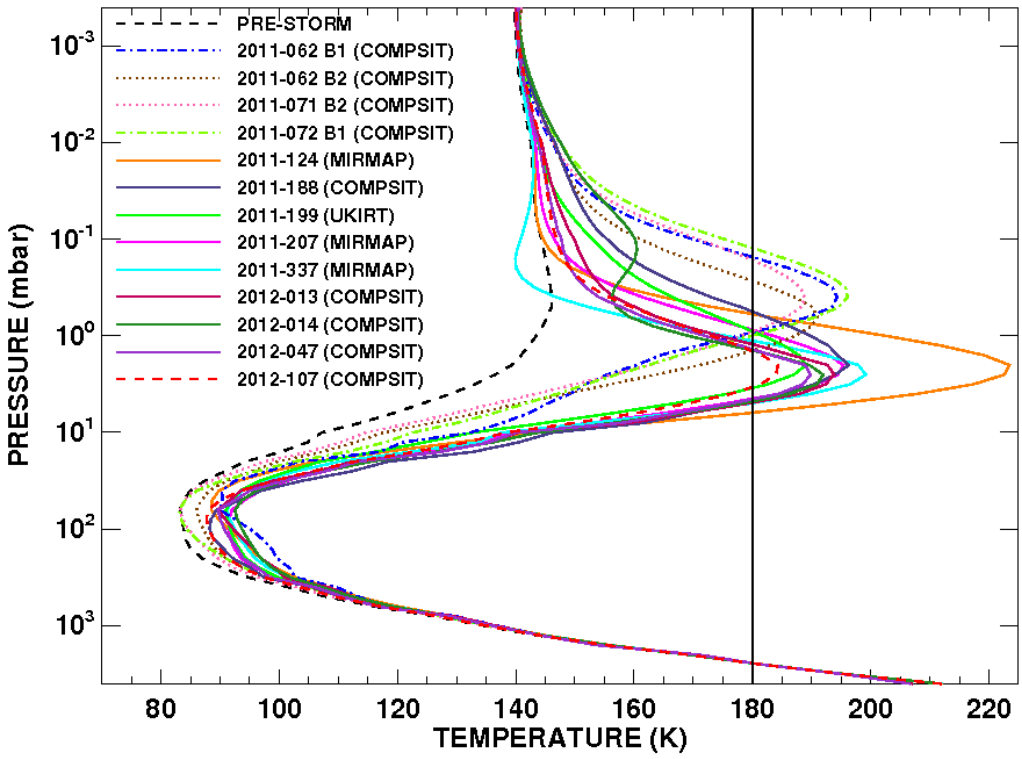

Figure 5: The temperature profiles retrieved from the CIRS observations for all of the observations given in Table 1. Also included is the temperature profile used for the UKIRT data set (green solid curve). The pre-storm time period is shown by the black-dashed curve. The first phase of the storm had two beacons and they are shown by the dash-dot and the dotted curves. Solid curves indicate the second phase of the storm when there was 1 beacon. The red dashed curve shows the temperature profile when ethylene was no longer present in the CIRS data. The vertical line indicates a threshold temperature above which ethylene emission "turned-on".

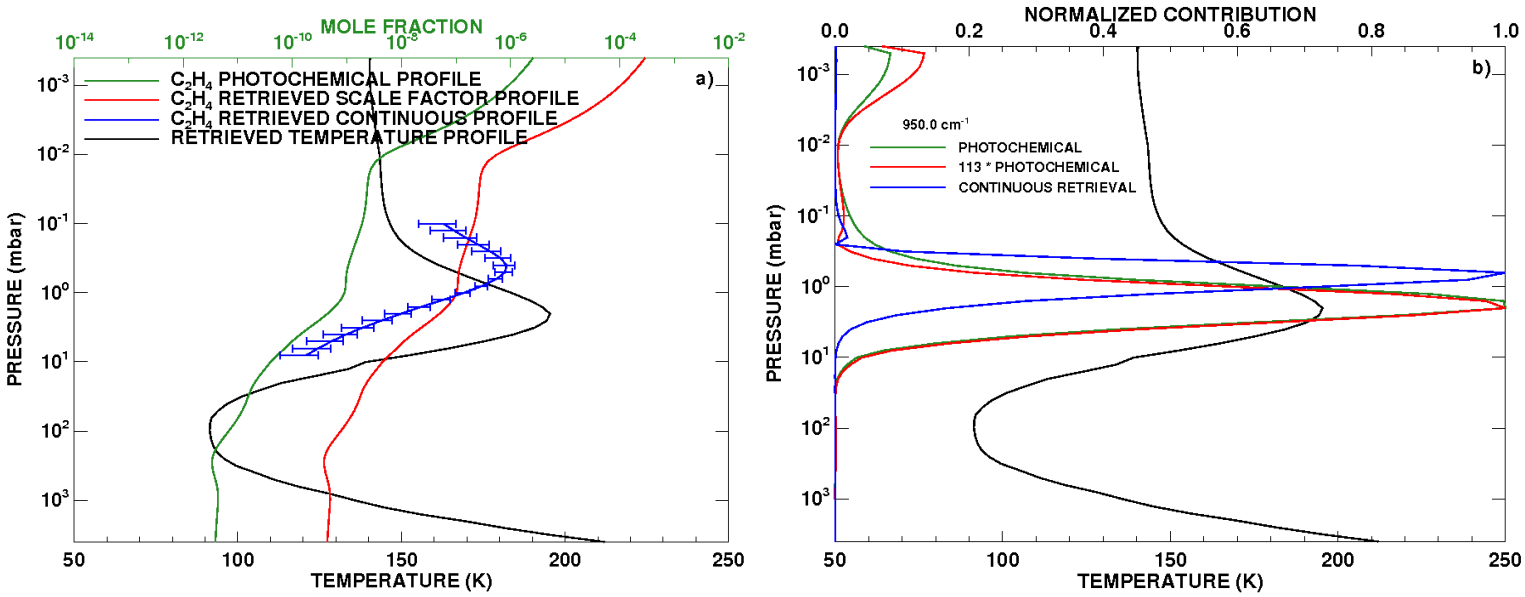

Figure 6: a) Retrieved profiles (temperature and abundance) from the July 26, 2011 MIRMAP observation at 2.5 cm^{-1} resolution. The temperature profile is shown in black. The C_2H_4 photochemical profile is in green. The red curve shows the resulting abundance profile when the scale factor approach is used in fitting the data. The blue curve shows the resulting abundance profile when using a profile that is allowed to vary continuously over the altitudes to which these data are sensitive. b) The contribution functions for the 3 abundance profiles shown in a) at 2.5 cm^{-1}.

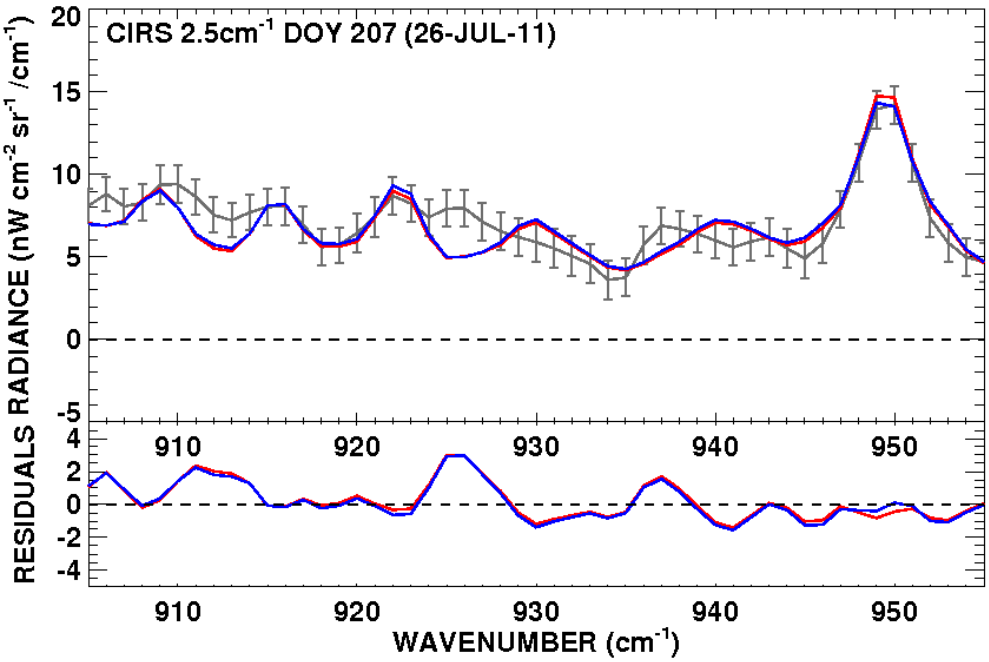

Figure 7: The 2.5 cm^{-1} data (black curve) and models (colored curves; red is scale factor, blue is continuously-variable) based on the abundance profiles shown in Fig. 6. The residuals between the models and data are shown in the bottom plot. Both of the retrieved profiles shown in Fig. 6 fit the 2.5 cm^{-1} spectrum with equivalent goodness-of-fits.

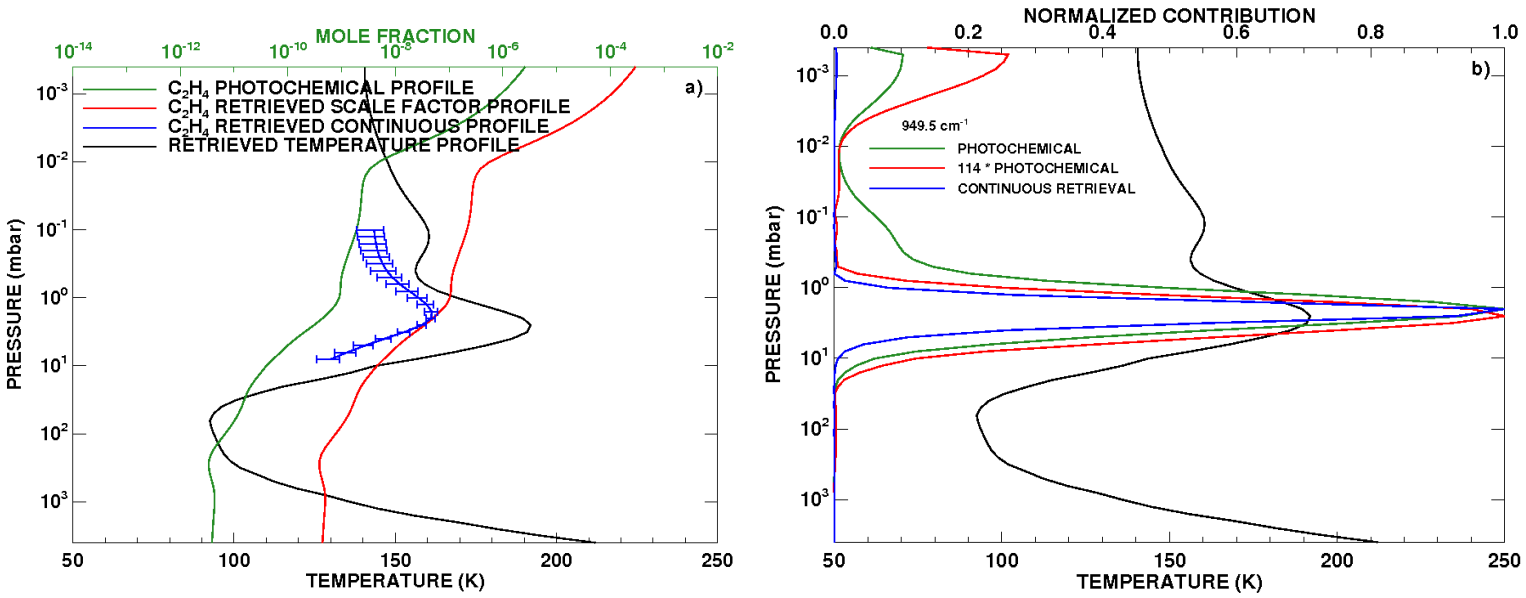

Figure 8: a) Retrieved profiles (temperature and abundance) from the January 14, 2012 COMPSIT observation at 0.5 cm^{-1} resolution. The temperature profile is shown in black. The C_2H_4 photochemical profile is in green. The red curve shows the resulting abundance profile when a scale factor approach is used in fitting the data. The blue curve shows the resulting abundance profile when using a profile that is allowed to vary continuously over the altitudes to which these data are sensitive. b) The contribution functions for the 3 abundance profiles shown in a) at 0.5 cm^{-1}.

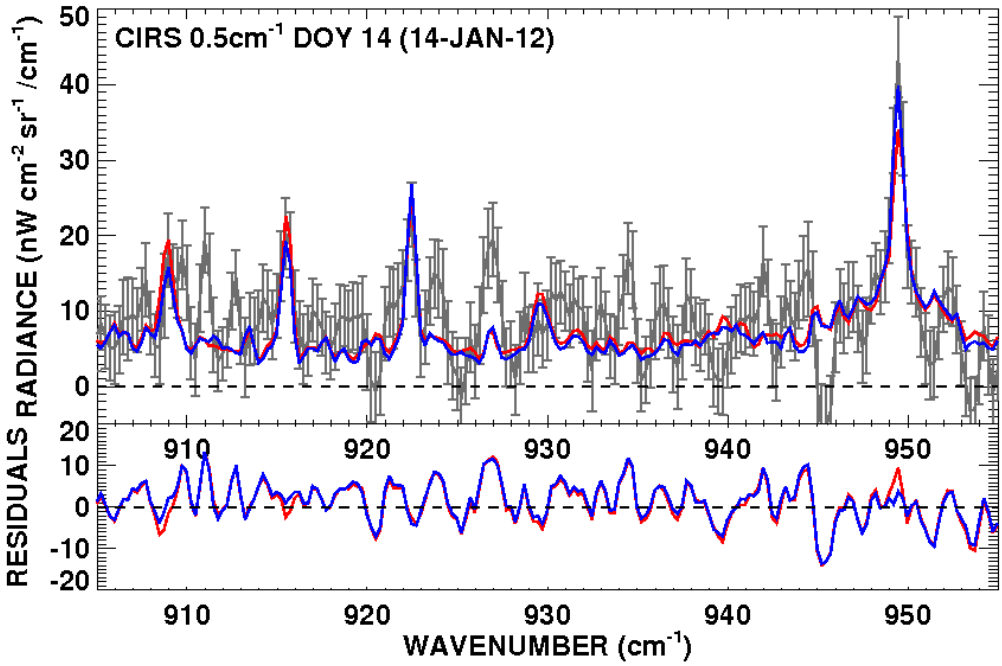

Figure 9: The 0.5 cm^{-1} data (black curve) and models (colored curves) based on the abundance profiles shown in Fig. 8. The residuals between the models and data are shown in the bottom plot. At this higher spectral resolution it is clear that the model produced from the continually varying abundance profile (blue curve) produces an overall better fit the to the main ethylene line at 949.5 cm^{-1}.

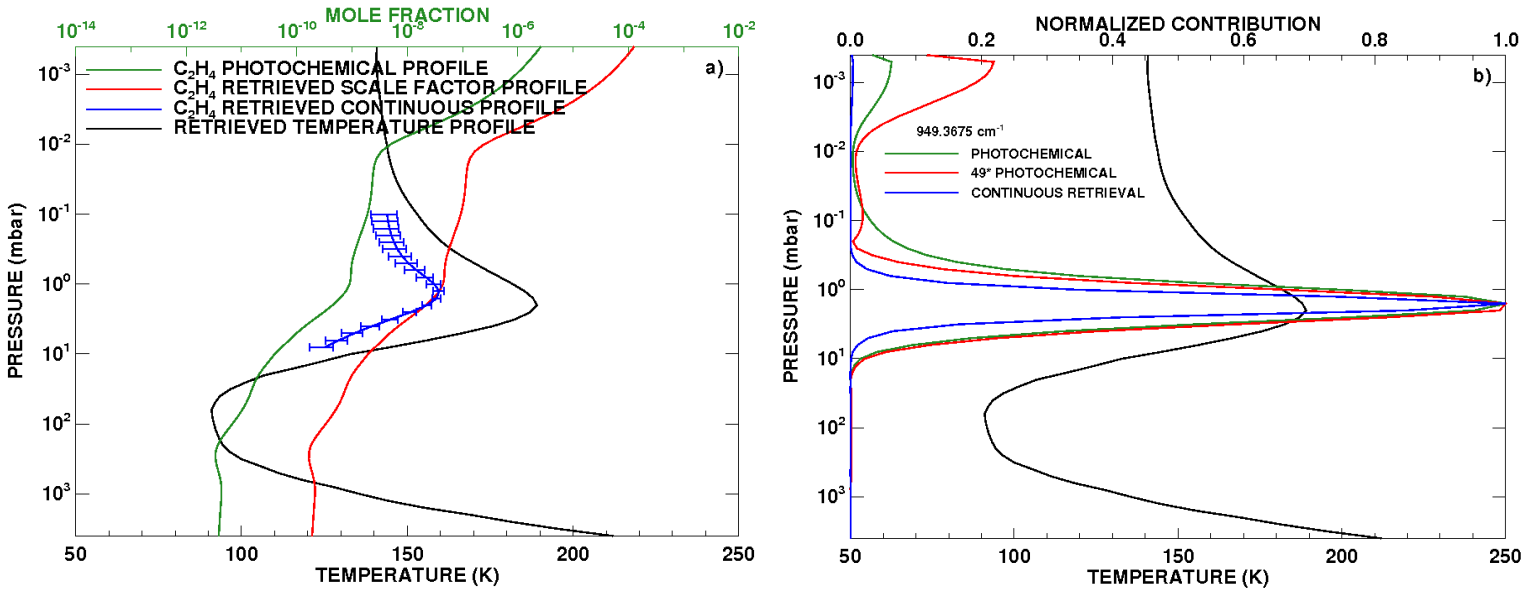

Figure 10: a) Retrieved profiles (temperature and abundance) from the July 18, 2011 UKIRT observation at 0.1 cm^{-1} resolution. The temperature profile is shown in black. The C_2H_4 photochemical profile is in green. The red curve shows the resulting abundance profile when a scale factor approach is used in fitting the data. The blue curve shows the resulting abundance profile when using a profile that is allowed to vary continuously over the altitudes to which these data are sensitive. b) The contribution functions for the 3 abundance profiles shown in a) at 0.1 cm^{-1}.

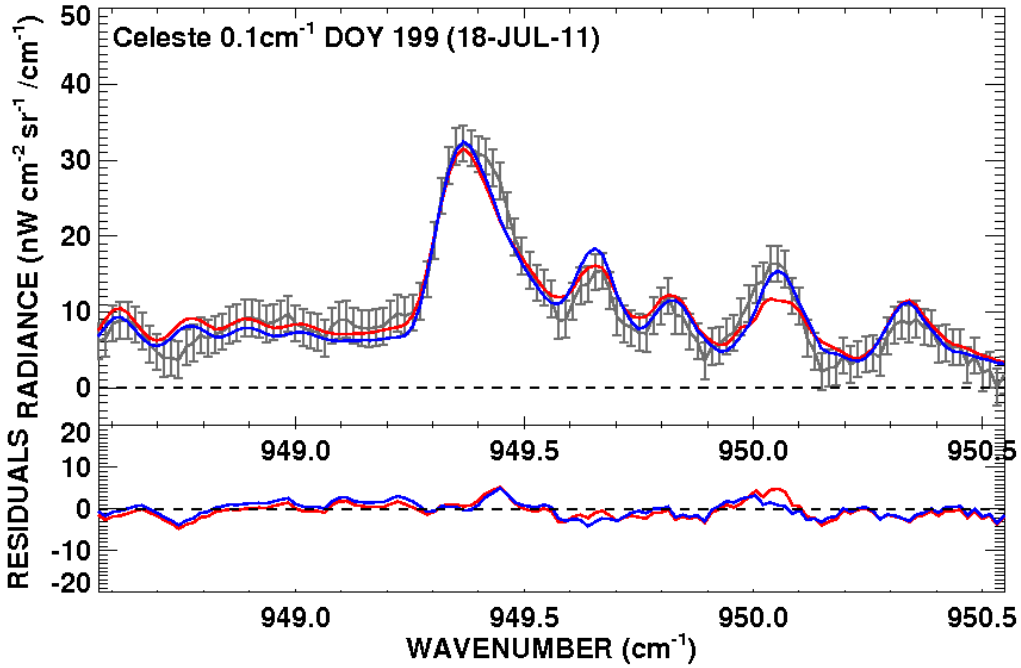

Figure 11: The 0.1 cm^{-1} data (black curve) and models (colored curves) based on the abundance profiles shown in Fig. 10. The residuals between the models and data are shown in the bottom plot. At this higher spectral resolution the continually varying abundance profile (blue curve) produces a better χ^2 than the scale factor model (red curve).

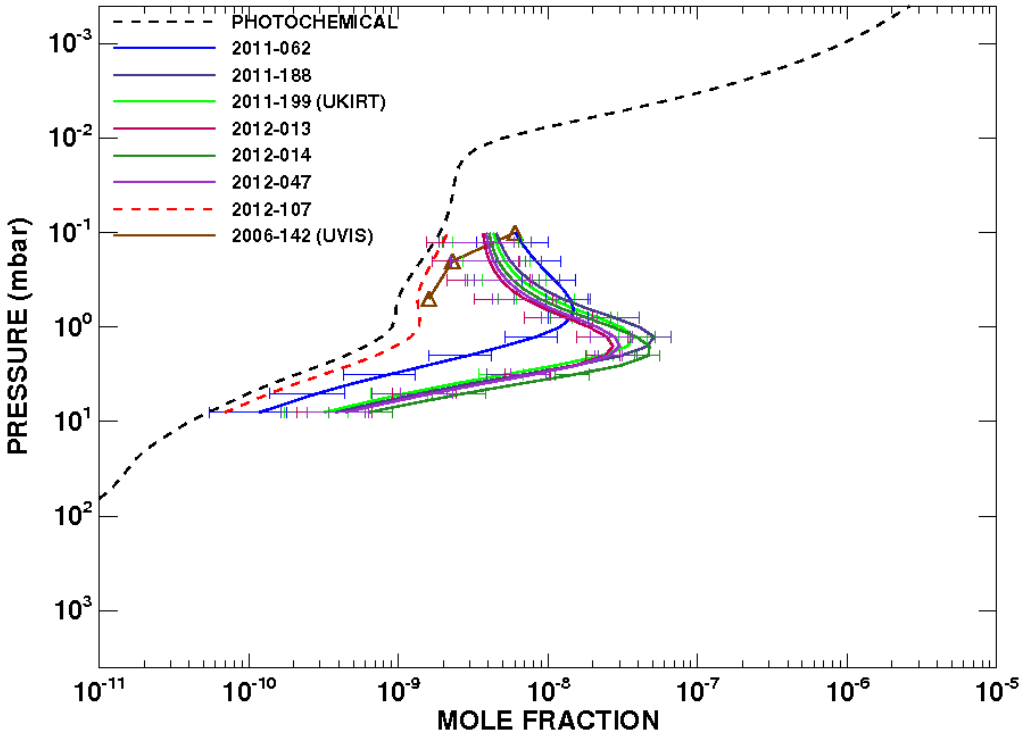

Figure 12: The C_2H_4 profiles retrieved from the CIRS 0.5 cm^{-1} (COMPSIT) and the UKIRT 0.1 cm^{-1} data. The ethylene abundance as measured by UVIS in pre-storm conditions is shown by the brown triangles. Observations with resolutions higher than 2.5 cm^{-1} were used to retrieve continuously-variable profiles. The black-dashed curve is the photochemical profile and the red-dashed curve is the fit produced by NEMESIS where the ethylene lines are not measurable above the noise.

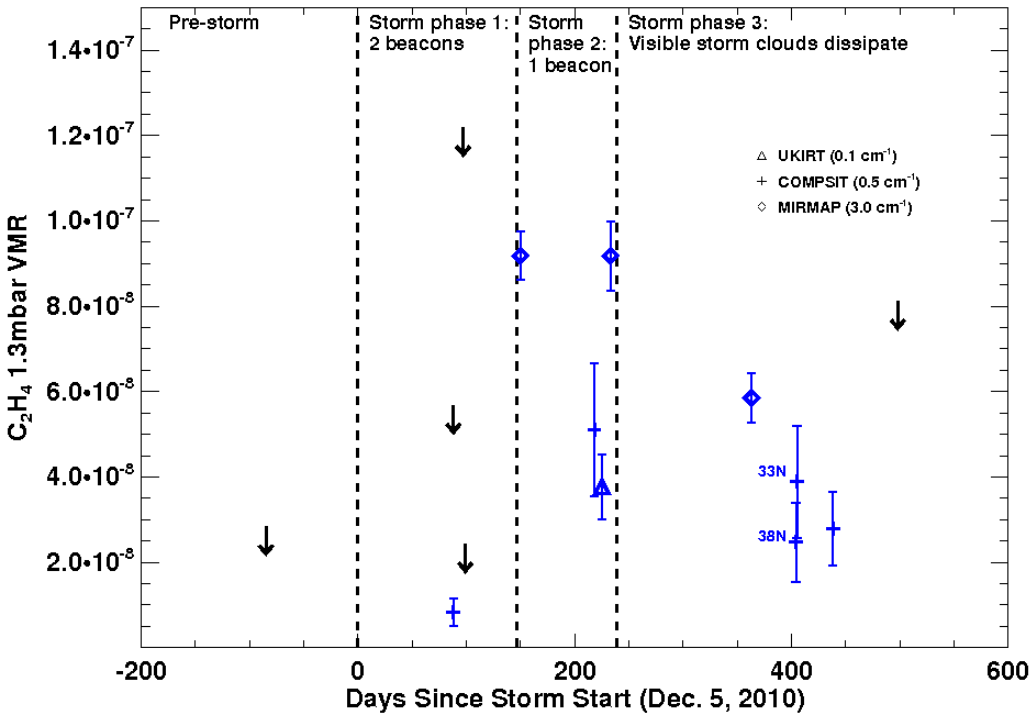

Figure 13: The retrieved C_2H_4 1.3 mbar volume mixing ratio values for all observation days. Data points in black without error bars show upper limits. Results from retrievals using CIRS at 3.0 cm^{-1} (MIRMAPs) data are shown with diamonds and using 0.5 cm^{-1} (COMPSITs) are shown with plus signs. A triangle displays the retrieved result from the ground-based 0.1 cm^{-1} UKIRT data. Upper limits were retrieved by looking at 3σ error bars on the ethylene spectrum.

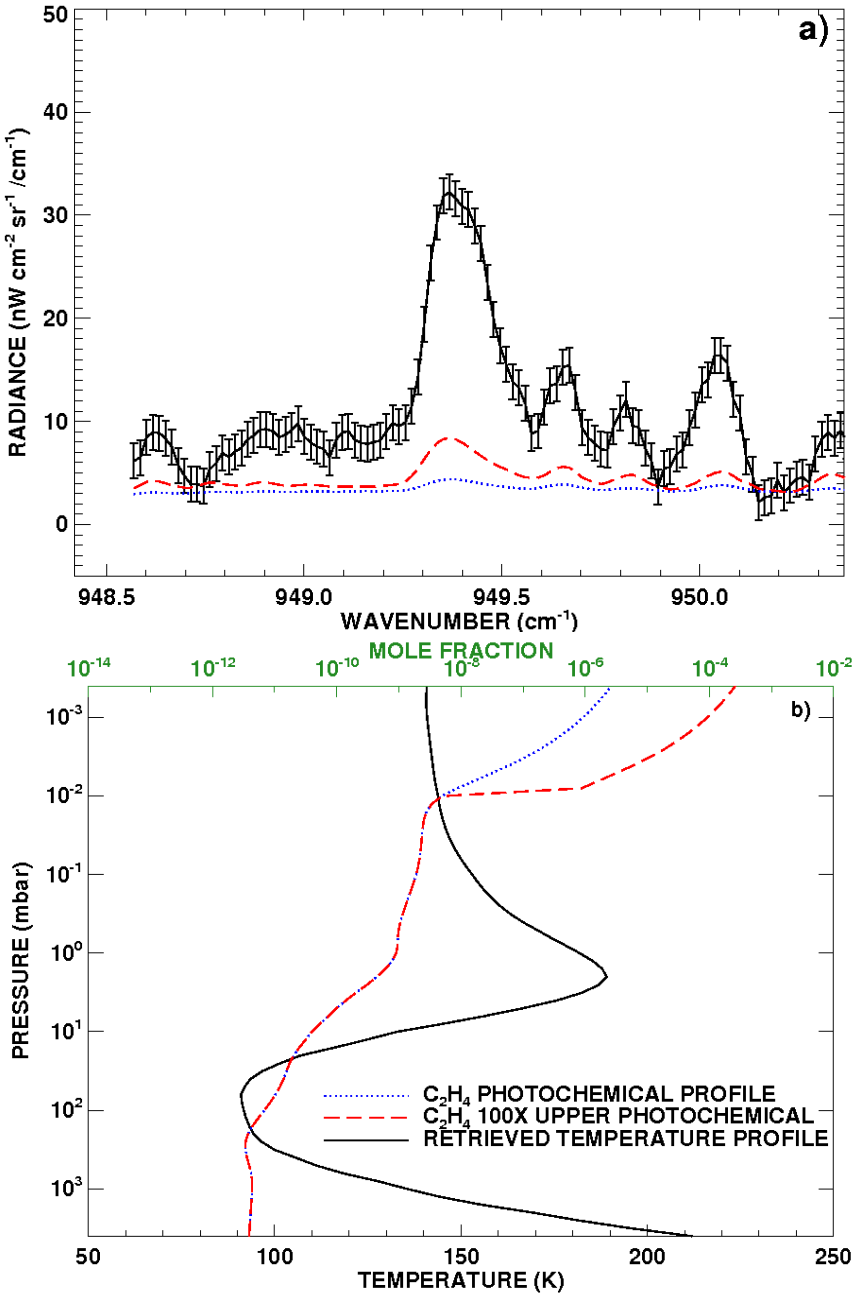

Figure 14: a) The 0.1 cm^{-1} UKIRT Celeste data (black curve) and models (colored curves) based on the abundance profiles shown (b). b) The temperature profile for the approximate time and spatial extent of the UKIRT observations is shown as the black curve. The blue dotted curve is the photochemical profile of C_2H_4 and the red dashed curve is 100x the photochemical profile at pressures less than 0.01 mbar.